



# Cortical Zinc Signaling Is Necessary for Changes in Mouse Pupil Diameter That Are Evoked by Background Sounds with Different Contrasts

 Patrick Cody,<sup>1,2,3</sup> Manoj Kumar,<sup>1</sup> and  Thanos Tzounopoulos<sup>1,3</sup>

<sup>1</sup>Department of Otolaryngology, Pittsburgh Hearing Research Center, University of Pittsburgh, Pittsburgh, Pennsylvania 15261, <sup>2</sup>Department of Bioengineering, University of Pittsburgh, Pittsburgh, Pennsylvania 15260, and <sup>3</sup>Center for the Neural Basis of Cognition, University of Pittsburgh, Pittsburgh, Pennsylvania 15213

Luminance-independent changes in pupil diameter (PD) during wakefulness influence and are influenced by neuromodulatory, neuronal, and behavioral responses. However, it is unclear whether changes in neuromodulatory activity in a specific brain area are necessary for the associated changes in PD or whether some different mechanisms cause parallel fluctuations in both PD and neuromodulation. To answer this question, we simultaneously recorded PD and cortical neuronal activity in male and female mice. Namely, we measured PD and neuronal activity during adaptation to sound contrast, which is a well-described adaptation conserved in many species and brain areas. In the primary auditory cortex (A1), increases in the variability of sound level (contrast) induce a decrease in the slope of the neuronal input–output relationship, neuronal gain, which depends on cortical neuromodulatory zinc signaling. We found a previously unknown modulation of PD by changes in background sensory context: high stimulus contrast sounds evoke larger increases in evoked PD compared with low-contrast sounds. To explore whether these changes in evoked PD are controlled by cortical neuromodulatory zinc signaling, we imaged single-cell neural activity in A1, manipulated zinc signaling in the cortex, and assessed PD in the same awake mouse. We found that cortical synaptic zinc signaling is necessary for increases in PD during high-contrast background sounds compared with low-contrast sounds. This finding advances our knowledge about how cortical neuromodulatory activity affects PD changes and thus advances our understanding of the brain states, circuits, and neuromodulatory mechanisms that can be inferred from pupil size fluctuations.

**Key words:** auditory cortex; contrast gain control; pupil diameter; zinc signaling

## Significance Statement

Changes in pupil diameter (PD) can track changes in alertness, attention, and mental effort. Our studies demonstrate that sound contrast-dependent changes in evoked PD require cortical neuromodulatory zinc signaling. As such, our results broaden our understanding of the relationship between neuromodulatory systems and changes in PD and offer a window for looking into mechanisms associated with distinct waking brain states. Given the correlation of waking states with fundamental cognitive functions, such as perception and learning, our findings provide a deeper understanding of the neuromodulatory mechanisms that transform changes in sensory input into altered cognition and behavior, which is a fundamental question in modern neuroscience.

Received May 22, 2023; revised Dec. 29, 2023; accepted Jan. 14, 2024.

Author contributions: P.C., M.K., and T.T. designed research; P.C. and M.K. performed research; P.C. contributed unpublished reagents/analytic tools; P.C. and M.K. analyzed data; P.C. and T.T. wrote the paper.

We thank Dr. Ross Williamson for his critical reading of the manuscript. For their keen critical feedback, we thank Drs. TK Kozai, Sandra Kuhlman, Srivatsun Sadagopan, and Matthew Smith. This work was supported by NIH Grants T32-DC011499 (to P.C.) and R01-DC019618, R01-EB033172, and R01-DC020923 (to T.T.).

The authors declare no competing financial interests.

Correspondence should be addressed to Thanos Tzounopoulos at thanos@pitt.edu or Patrick Cody at pac94@pitt.edu.

<https://doi.org/10.1523/JNEUROSCI.0939-23.2024>

Copyright © 2024 the authors

## Introduction

Variations in luminance trigger fluctuations in pupil diameter (PD) that, in turn, regulate the amount of light entering the eyes. Although these variations are mainly mediated through the pupillary light reflex (Larson and Behrends, 2015; Joshi and Gold, 2020), this is not the only mechanism associated with PD fluctuations. In consistent luminance, many studies have shown that fluctuations in PD can track changes in alertness, attention, and mental effort (Zekveld et al., 2011, 2014, 2018; Reimer et al., 2014; Winn et al., 2015; van der Wel and van

Steenbergen, 2018; Joshi and Gold, 2020; Saderi et al., 2021). It is known that these PD fluctuations are heavily affected by locus ceruleus (LC) activity (Joshi et al., 2016; Liu et al., 2017; Privitera et al., 2020) and are highly correlated with changes in cortical adrenergic and cholinergic activity (Reimer et al., 2016). Thus, PD is often used as a measure of neuromodulation; so, it is important to better understand the causality or directionality of this correlation. PD additionally correlates with spontaneous single-neuron activity and membrane potential (Reimer et al., 2014; McGinley et al., 2015a), sensory responses of cortical sensory neurons (McGinley et al., 2015a; Lin et al., 2019; Schwartz et al., 2019), and behavioral performance (McGinley et al., 2015b; Saderi et al., 2021). Such physiological and neuromodulatory factors may contribute to—or be shaped by—transient (evoked) and/or baseline (spontaneous PD changes independent of experimental assays) PD fluctuations. In this context, neither the precise circuits and mechanisms nor the directionality of the different processing stages and neuromodulatory effects that are involved in these PD fluctuations are clearly understood (Joshi and Gold, 2020). Namely, are the fluctuations in neuromodulatory activity in a particular cortical area necessary for the observed fluctuations in PD? Or is it that some different mechanisms cause parallel fluctuations in both PD and neuromodulation and thus associations between PD and neuromodulatory signaling are not dependent on each other? Understanding these relationships between central neuromodulatory mechanisms and PD fluctuations will offer a window for looking into mechanisms associated with distinct brain waking states in mice, nonhuman primates, and humans. Given the correlation of waking states with fundamental cognitive functions (Joshi and Gold, 2020), such as perception and learning, a deeper understanding of the neuromodulatory mechanisms that transform changes in sensory input into altered cognition and behavior is a key question in modern neuroscience.

To explore the links between neuromodulatory mechanisms, cortical sensory adaptation, and PD fluctuation, we studied a form of cortical sensory adaptation and its effect on PD. Importantly, we evaluated the effects of blocking a cortical neuromodulatory mechanism, which disrupts this sensory adaptation, on PD responses. Namely, we used adaptation to sound contrast, termed contrast gain control (CGC), which is a well-described sensory adaptation conserved in many species and brain areas (Rabinowitz et al., 2011; Lohse et al., 2020). Increases in the variability of sound level (contrast) induce a decrease in the slope of the neural input–output relationship, a gain reduction, to efficiently maintain stimulus discriminability (Willmore et al., 2014; Angeloni et al., 2021). Here, we found that high-contrast sounds evoke larger increases in PD compared with low-contrast sounds. Moreover, we know that the adaptation of A1 neurons to changes in sound contrast depends on cortical neuromodulatory synaptic zinc signaling, which selectively suppresses cortical neural responses to sound in high contrast (Cody and Tzounopoulos, 2022). Synaptic zinc is a neuromodulator that is coreleased with glutamate and GABA and modulates NMDA, AMPA, and GABA<sub>A</sub> postsynaptic currents in an activity-, cell-, and synapse-specific manner (Ruiz et al., 2004; Paoletti et al., 2009; Vergnano et al., 2014; Anderson et al., 2015; Kouvaros et al., 2020, 2023; Krall et al., 2020; Vogler et al., 2020; Morabito et al., 2022; Bender et al., 2023). Through these actions, synaptic zinc modulates cortical auditory, visual, and somatosensory sensory processing in a stimulus- and context-dependent manner (Brown and Dyck, 2002; Dyck et al., 2003; Anderson et al., 2017; McAllister and Dyck, 2017;

Wu and Dyck, 2017; Kumar et al., 2019; Cody and Tzounopoulos, 2022). Thus, we reasoned that by selectively targeting cortical zinc signaling during sound contrast adaptation, we will have a unique opportunity to interrogate how cortical neuromodulatory mechanisms contribute to PD fluctuations during sensory adaptation.

To address the potential hierarchy (directionality) of the associations between PD and cortical neuromodulation, we simultaneously recorded PD and cortical neural activity during sensory adaptation. We first assessed PD fluctuations before (baseline) and then during low and high-contrast sound stimuli (evoked). We found that high-contrast sounds evoke larger increases in PD compared with low-contrast sounds. To explore whether changes in PD are controlled by cortical neuromodulatory zinc signaling during this adaptation, we imaged single-cell neural activity in the primary auditory cortex (A1), manipulated cortical synaptic zinc signaling, and assessed PD in the same awake mouse. We discovered a previously unknown cortical neuromodulatory mechanism that is necessary for sound contrast-dependent changes in PD. Our results advance how activity in different neuromodulatory systems affects changes in PD and how brain state, as evidenced by transient PD changes, is conveyed via cortical zinc signaling.

## Materials and Methods

**Animals.** We used four female (F) and four male (M) C57BL6/J mice (The Jackson Laboratory strain #000664) for the experiments presented in Figures 1, 2*a–c*, and 3. For Figure 2*a–e*, we used six F and eight M C57BL6/J mice. For Figures 4, *b* and *d*, and 6*d*, we used three F and three M mice with homozygous lack of the vesicular zinc transporter [ZnT3 (Cole et al., 1999)], ZnT3-KO mice. For Figure 5, we used one F and two M C57BL6/J mice. For Figure 4, *a* and *c*, we used six F and four M homozygous littermate controls, ZnT3-WT mice. ZnT3-KO and ZnT3-WT mice were considered congenic with C57BL6/J mice as they were backcrossed with C57BL6/J mice from the founder line (The Jackson Laboratory strain #005064). Experiments using ZnT3-WT/KO mice were done blind to KO or WT designation. We used an additional three M and one F C57BL6/J mice for ACSF control experiments in Figure 6. Mice were handled, anesthetized, and killed according to methods approved by the University of Pittsburgh Institutional Animal Care and Use Committees (IACUC). The approved IACUC protocol numbers that were employed for this study were 17071036 and 17127808.

**Stereotaxic adeno-associated virus injection.** At P24–P30, mice were injected with an adeno-associated virus (AAV), AAV9.CaMKII.GCaMP6f.WPRE.SV40 (Addgene 100834;  $2\text{--}2.5 \times 10^{13}$  GC/ml; diluted at 1:6 in phosphate-buffered saline), into the right auditory cortex (ACtx) to express GCaMP6f in putative principal cells expressing the calcium-/calmodulin-dependent protein kinase 2 (CaMKII) as described previously (Cody and Tzounopoulos, 2022) in preparation for *in vivo* calcium imaging.

**Acute surgery preparation for *in vivo* imaging.** At P38–P49, mice underwent craniotomy surgery over the right ACtx and were secured to the microscope apparatus for imaging experiments as described previously (Cody and Tzounopoulos, 2022). Due to the surgical preparation for imaging the right ACtx, the right ear was mostly occluded. Mice were situated on the microscope stage such that the right pupil was visible to a pupillometry camera, and the left pupil was in view of a UV LED light for maintaining constant pupil size (see “Pupillometry: acquisition” in Materials and Methods).

**Sound stimulus delivery.** Sound stimuli were delivered from a free-field speaker (ES1, Tucker-Davis Technologies) situated 10 cm from the animal's left ear, as described previously (Cody and Tzounopoulos,

2022). Output voltage for the frequencies comprising the dynamic random chord (DRC) and pure-tone stimuli (see “DRC sound stimuli” and “CGC assay” in *Materials and Methods*) was scaled according to speaker calibration data to account for a nonlinear speaker frequency response. The speaker was calibrated using microphones with attached preamps (1/8 in. 4138-A-015 and 1/4 in. 4954-B, Brüel & Kjær) that were calibrated to a 1 kHz pure tone at 94 dB SPL from a reference sound calibrator (Type 4231, Brüel & Kjær). Sound signals were converted to analog output at 250 kHz (USB-6229, National Instruments) and sent to the ES1 speaker via an ED1 speaker driver (Tucker-Davis Technologies).

#### *Widefield epifluorescence imaging and analysis for A1 localization.*

Widefield (WF) epifluorescence imaging of GCaMP6f fluorescence responses was used to localize A1 for two-photon calcium imaging (2PCI) as described previously (Cody and Tzounopoulos, 2022). Briefly, we presented 5–6 kHz and 12 kHz pure-tone stimuli at 60 dB SPL to map tonotopic gradients (Linden et al., 2003; Anderson et al., 2017). We imaged GCaMP6f fluorescence under a 4× objective (Olympus) through a GFP filter (BrightLine GFP-A-Basic, Semrock) using a cooled CCD camera (Retiga 2000R, Q-Imaging) at a 20 Hz frame rate with a 200×150 pixel resolution and 8× spatial binning. Fluorescence responses were calculated as normalized change from the prestimulus baseline ( $F_0$ ) at each pixel ( $\Delta F/F = (F - F_0)/F_0$ ). The prestimulus baseline was calculated from a 1 s average of fluorescence intensity prior to pure-tone onset (at 2–3 s during imaging). Responses to the 5–6 kHz pure tones reveal two salient low-frequency regions of ACtx. In combination with responses to the 12 kHz pure tone, which are evident between the two low-frequency regions, the tonotopic axis of primary auditory cortex (A1) and anterior auditory field can be anatomically identified based upon their mediolateral and dorsoventral positioning (Linden et al., 2003; Anderson et al., 2017).

**DRC sound stimuli.** Low and high sound level contrast DRC stimuli were generated with the same mean sound level. DRCs consisted of 28 pure-tone frequencies between 5 and 51.874 kHz at one-eighth octave intervals. For each 25 ms DRC, sound levels for low-contrast DRC were sampled from a narrow uniform distribution between 50 and 60 dB SPL ( $\pm 5$  dB;  $\sigma_L \approx 2.9$  dB SPL), while sound levels for high-contrast DRC were sampled from a wider distribution between 40 and 70 dB SPL ( $\pm 15$  dB;  $\sigma_L \approx 8.7$  dB SPL). Both distributions had the same 55 dB SPL mean. Overall stimulus intensity was  $84.4 \pm 0.6$  dB SPL for low contrast and  $87.8 \pm 1.5$  dB SPL for high contrast. The average intensity difference between stimuli (3.4 dB SPL) is comparable to previous studies (Rabinowitz et al., 2011; Lohse et al., 2020). For CGC analyses, DRC stimuli included a 70 dB pure tone at 2 s. In this case, the DRC amplitude was set to 0 V for 400 ms, and a 70 dB SPL pure tone lasting 400 ms was inserted within this gap. For sound-evoked pupil response analyses, DRC stimuli did not include a pure tone.

**2PCI.** Sound-evoked responses from putative principal cells expressing CaMKII in the right ACtx were imaged with 2PCI as described previously (Cody and Tzounopoulos, 2022). We collected  $145 \times 145$   $\mu\text{m}$  images at  $256 \times 256$  pixel resolution at an effective frame rate of 5 Hz. For analyses of cell calcium responses, we used custom MATLAB scripts to draw ellipses around all nonoverlapping cells in the plane having a visible “doughnut”-shaped fluorescence signal. Raw fluorescence intensity for each cell across time was calculated from the mean fluorescence intensity signal within ellipse bounds at each image frame.

**Pupillometry: acquisition.** Video of the animal's right pupil was recorded 4 s prior to sound onset and continued for the duration of each 2PCI imaging trace. A UV LED (375 nm, 2.5 mW, Thorlabs) directed into the animal's left eye maintained both animal's pupils at the midsize range in the dark recording chamber to optimize dynamic range for baseline PD and sound-evoked PD changes (see “Pupillometry: analysis” in *Materials and Methods*). UV intensity was set with an LEDD1B driver (Thorlabs) via a voltage divider circuit

(470  $\Omega$  rated at 25 W, Mouser Electronics) and was kept at constant luminance throughout the experiment. UV light was shielded from the 2PCI objective to avoid interference with the 2P photomultiplier tubes. Light spillover from the 2P laser through the animal's brain and into the pupil provided sufficient illumination for pupil imaging. Video frames were captured with a monochrome CMOS USB camera (DCC1545M; Thorlabs) behind a 1× telecentric lens and 380 nm cut-on UV filter (Edmund Optics). Frames were captured at 10 Hz, synchronized with 2P frame acquisition using an NI-DAQ board counter output channel, and time-stamped using a custom-written MATLAB function for ScanImage with a .NET camera API library (Thorlabs).

**ZX1 infusion.** Sound-evoked pupil responses were recorded before (control: CTRL) and after injecting 100  $\mu\text{M}$  ZX1 (a fast extracellular high-affinity zinc-specific chelator; Pan et al., 2011) solution ipsilateral to imaging in right ACtx (Figs. 2, 4). To control for the solution volume and presence of the injection pipette, responses were also recorded before and after injecting ACSF (Fig. 6b). Prior to imaging, we inserted a pulled glass micropipette just below the pial surface at the edge of the craniotomy within ACtx. The pipette contained 100  $\mu\text{M}$  ZX1 and 50  $\mu\text{M}$  Alexa Fluor 594 in ACSF (herein referred to as “ZX1 solution”) or just 50  $\mu\text{M}$  Alexa Fluor 594 in ACSF (herein referred to as “ACSF solution”) and was backfilled with mineral oil and connected to a 5  $\mu\text{l}$  glass syringe mounted in a motorized syringe pump (World Precision Instruments). After a minimum of 20 min following cessation of isoflurane, we recorded the baseline PD and sound-evoked PD. To infuse ZX1 contralateral to the imaging of the right ACtx, we implanted chronic cannulas in the left ACtx in mice as described previously (Kumar et al., 2019) and illustrated in Figure 5a. Twelve to 16 d after surgery, we imaged sound-evoked responses of right (ipsilateral) A1 principal neurons (PNs) in awake mice.

**Frequency response area mapping.** At the beginning of each 2PCI experiment, we mapped frequency response areas (FRAs) of the neurons in the imaging field as described previously (Cody and Tzounopoulos, 2022) to determine the pure-tone frequency to be used in the CGC assay (see “CGC assay” in *Materials and Methods*). Briefly, we presented pure tones (linearly ramped at 10 ms) comprising the DRC stimulus (5–51.874 kHz; see “DRC sound stimuli” in *Materials and Methods*) lasting 400 ms at intensities of 30, 50, and 70 dB SPL, occurring at 0.6 s or 1 s within a 3 s interstimulus-interval window. Fluorescence responses to sound stimuli were calculated as normalized fluorescence change from the prestimulus baseline ( $\Delta F/F = (F - F_0)/F_0$ ). For FRA mapping, prestimulus baseline ( $F_0$ ) was calculated as the average cell fluorescence signal ( $F$ ) across a 600 ms baseline prior to pure-tone onset. Solely cells with significant pure-tone responses were included in analyses, that is, cells where the trace average of the maximum  $\Delta F/F$  value within an 800 ms window following pure-tone onset is  $\geq 2$  standard deviations above the trace average of  $F_0$ . During each experiment, we performed an ad hoc analysis to quickly determine the pure-tone frequency that elicits the maximum  $\Delta F/F$  response across an average of all cell FRAs collapsed across stimulus intensity. This pure-tone frequency was then used for the CGC assay.

**CGC assay.** For each experiment, a given pure-tone frequency (as determined during ad hoc FRA mapping; see previous section) was presented in each contrast (low, high) combination in a pseudorandom fashion. For each imaging trace, the DRC sound stimulus was both preceded and followed by 4 s of silence. Traces were interleaved by laser and sound-off periods of pseudorandom duration lasting 25–35 s. A minimum of eight repetitions of each contrast was presented.

**2PCI processing and analysis.** For each experiment, nonrigid motion correction of the 2PCI frames was performed using the NoRMCorre MATLAB toolbox (Pnevmatikakis and Giovannucci, 2017). Neuropil contamination was assessed using the FISSA Python toolbox (Keemink et al., 2018), scaled by 0.8 (Kerlin et al., 2010; Chen et al., 2020), and removed to obtain motion- and neuropil-corrected average fluorescence intensity across time for each cell. Normalized baseline subtracted

fluorescence traces ( $F(t) = \Delta F/F$ ) were first calculated as  $(F - F_{0\_DRC})/F_{0\_DRC}$ , where  $F_{0\_DRC}$  is the average cell fluorescence intensity before DRC sound onset across  $-1.2$  to  $0$  s. To quantify responses to pure tones that were preceded by 2 s of contrast DRC, we calculated  $F(t) - F_{0\_PT}$ , where  $F_{0\_PT}$  is the average of  $F(t)$  across  $1-2$  s for a 2 s DRC duration. Inclusion criteria: solely nonoverlapping cells deemed tone responsive were included. For CGC analyses, solely cells that were significantly responsive to pure tones in both low and high contrast were included. We used a tone sensitivity index,  $d'$ , to identify tone-responsive cells ( $d' \geq 0$ ) as described previously (Romero et al., 2019). Cells were deemed significantly responsive to pure tones if the average trace maximum  $\% \Delta F/F$  value within an 800 ms window following pure-tone onset was  $\geq 2$  standard deviations (2 SD) above the trace average baseline  $\% \Delta F/F$ . The baseline  $\% \Delta F/F$  is the average of  $\% \Delta F/F$  across  $1-2$  s.

Cells were grouped by animal in baseline PD bins to maintain pairing by contrast condition. To quantify CGC, we calculated the contrast scaling factor, defined as the population mean of individual cell average peak responses in low divided by average peak responses in high contrast. Reliability was calculated as the average trial-to-trial zero lag cross-correlation of peak pure-tone response traces (at  $2-3.2$  s) for all responses for a given cell and is presented as a population average.

**Pupillometry: analysis.** PD was obtained from pupil videos using a least squares circle fit to dots fitted to pupil perimeter using a DeepLabCut convolutional neural network model (Mathis et al., 2018; Nath et al., 2019) along with custom-written MATLAB and Python scripts. Pupil videos with dropped frames were realigned to frame time stamps. Using DeepLabCut, we trained a 101-layer ResNet model with default augmentation on 11 videos from different experiments that were labeled with eight dots around the pupil perimeter (Mathis et al., 2018). For each frame from model analyzed videos, a minimum of three dots at  $>0.9$  likelihood were needed to fit a circle via least squares else the frame was discarded. Pupil (circle) diameter traces were processed sequentially by first removing  $>6$  SD outlier frames from the first derivative, next linearly interpolating missing time points with the previous two and following two adjacent time points, and finally filtering the trace with a third order 3 Hz low-pass Butterworth filter (Mridha et al., 2021).

Evoked pupil responses are presented as percent baseline PD: for each PD trace, PD was divided by average PD prior to sound onset (baseline PD;  $-4$  to  $0$  s) and then multiplied by 100. For responses binned by percent baseline PD, PD traces for each animal were first calculated as a percentage of the animal's maximum PD during the experiment. These traces were then averaged across the baseline epoch ( $-4$  to  $0$  s) and then grouped in seven bins. The last bin ( $>76\%$ ) was wider to accommodate fewer samples in that PD range. 2PCI data in each of these bins correspond to an average of cell average traces occurring at a given pupil bin.

We limited sound-evoked pupil response analyses to responses with a baseline PD at  $<50\%$  of animal max PD (50th percentile) for several reasons. First, at relatively dilated states, the pupil tends to constrict (de Gee et al., 2014; Mridha et al., 2021), and evoked pupil responses are significantly negatively correlated with baseline PD (data not shown;  $r_{(624)} = -0.35$ ,  $p = 1.20 \times 10^{-19}$ ). At PDs  $<50\%$  of maximum animal PD, this correlation becomes much smaller and is no longer significant (Fig. 6*b*;  $r_{(382)} = -0.055$ ,  $p = 0.285$ ). Additionally, because we are interested in the contribution of cortical CGC to pupil responses, we focused on the 50th percentile where CGC is strongest (Fig. 1*h*).

We used a linear mixed-effects (LME) model to analyze whether baseline and/or evoked PD is predictive of cell peak pure-tone responses (Fig. 3). We assessed fixed effects of contrast and random-intercept effects of subject, baseline PD, and evoked PD using a coefficient test (Fig. 3*a*). The model in Wilkinson notation (Wilkinson and Rogers, 1973; Pinheiro and Bates, 2000) is as follows:  $\text{peakPureToneResponse} \sim \text{baseline\_PD} + \text{contrast} \times \text{pupil\_at\_1-2 s} + (1 \mid \text{subject}) + (1 \mid \text{baseline\_PD}) + (1 \mid \text{pupil\_at\_1-2 s})$ . We used a likelihood ratio test between the full model and a null model to determine whether the full model improves pure-tone response prediction over the null model, which solely includes baseline PD as a predictor. The null model in Wilkinson notation is as follows:  $\text{peakPureToneResponse} \sim \text{baseline\_PD} + (1 \mid \text{subject}) + (1 \mid \text{baseline\_PD})$ .

We used growth curve analysis (GCA; Mirman, 2016; Montes-Lourido et al., 2021) to quantitatively compare evoked PD between contrast and drug treatment conditions. For this analysis, we fit orthogonal first- and second-order time polynomials to pupil responses (from sound onset to 2 s post onset) and separately assessed their interaction with fixed effects of contrast and drug treatment using an LME model. We included random subject-level intercept effects to account for variability between mice. GCA precludes bias associated with choosing analysis windows and captures PD evolution over time (slope) via the fitted first-order polynomial (Montes-Lourido et al., 2021). The LME model in Wilkinson notation (Wilkinson and Rogers, 1973; Pinheiro and Bates, 2000) is as follows:  $\text{pupil} \sim (\text{tPoly1} + \text{tPoly2}) \times \text{contrast} + (\text{tPoly1} + \text{tPoly2}) \times \text{treatment} + (1 \mid \text{subject})$ . For comparing control high-contrast responses between ZnT3-WT and ZnT3-KO genotypes, we used a simpler LME model:  $\text{pupil} \sim (\text{tPoly1} + \text{tPoly2}) \times \text{genotype} + (1 \mid \text{subject})$ . tPoly1 and tPoly2 are the first- and second-order orthogonal time polynomials; their coefficients correspond to slope and acceleration GCA weight/coefficient estimates. The MATLAB "fitlme" function was used to calculate coefficients and standard errors. These were confirmed with the "lmer" function in R. Tukey adjusted pairwise comparisons were done using the "emmeans" function in R with a Satterthwaite correction for large degrees of freedom.

**Statistics.** For grouped single-factor data that reject the Anderson-Darling null hypothesis test for normality, we used a one-way Kruskal-Wallis test (Fig. 1*f-h*). We analyzed grouped two-factor cell response data with a two-way ANOVA (Fig. 1*i*). We used a coefficient test and likelihood ratio test on LME models to assess whether baseline and/or evoked PD is predictive of cell peak pure-tone responses (Fig. 3). GCA was used to compare the initial rising phase ( $0-2$  s) of evoked pupil responses between conditions (Figs. 4, 6; as described in "Pupillometry: analysis" in Materials and Methods). Linear regression and Pearson's correlation coefficient were used to assess the relationship between baseline PD and experiment duration (Fig. 6*a*) and between magnitude evoked pupil response and baseline PD (Fig. 6*c*).

## Results

### CGC is more robust at intermediate baseline PD

Because the cortical gain is associated with PD (McGinley et al., 2015*a*; Schwartz et al., 2019), we first investigated whether CGC (Rabinowitz et al., 2011; Lohse et al., 2020; Angeloni et al., 2021) similarly varies in strength with baseline PD. To address this, we performed a 2PCI assay of sound CGC in ACTx (Cody and Tzounopoulos, 2022) and simultaneous pupillometry to measure PD (Fig. 1*a*). This experimental setup allowed us to interrogate whether PD prior to sound onset (baseline PD; Fig. 1*c,e*, gray box) is associated with CGC magnitude (Fig. 1*d*, representative cell from animal in *b,e*). Briefly, we presented a pure tone at 70 dB SPL following 2 s of DRCs having either low or high spectrotemporal sound level contrast (Fig. 1*c*). Sound level varied across both frequency and time at  $\pm 5$  dB ( $\sigma \approx 2.9$  dB) for low-contrast DRCs and  $\pm 15$  dB ( $\sigma \approx 8.7$  dB) for high-contrast DRCs, but both DRC stimuli had the same mean sound level of 55 dB. Simultaneously, we recorded both single-cell calcium responses using 2PCI (Fig. 1*b*, bottom panel, Fig. 1*d*) and PD using pupillometry (Fig. 1*b*, top panel, Fig. 1*e*).

Because pure-tone response amplitude is associated with PD (McGinley et al., 2015*a*; Lin et al., 2019), we first assessed potential associations between baseline PD and peak pure-tone response amplitude regardless of contrast. For each recorded field of cells, we chose the pure-tone frequency that elicited the largest response across an average of cell FRAs. In agreement with previous studies (McGinley et al., 2015*a*; Lin et al., 2019), we also observed an inverse  $U$  relationship, where pure-tone response amplitudes are largest at baseline PDs that are within

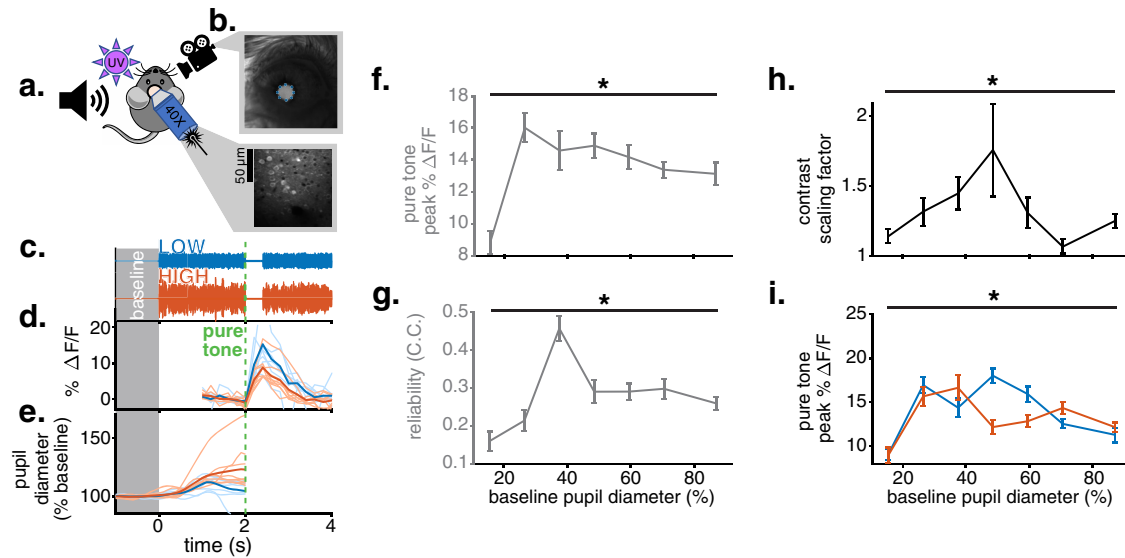


**Figure 1.** Baseline PD is associated with the magnitude of CGC. *a*, Schematic of preparation for simultaneous 2PCI and pupillometry. *b*, Top panel: representative image of mouse eye with pupil labels (blue) fitted by trained DeepLabCut model. Bottom panel: representative image of 2PCI field of view at  $145 \times 145 \mu\text{m}$  showing A1 L2/3 CaMKII expressing PNns. *c*, Representative sound voltage signals of low- (blue) and high- (orange) contrast DRC stimuli with a 400 ms pure tone occurring at 2 s (green dotted line). The gray box denotes the baseline epoch. *d*, *e*, Representative 2PCI and pupil traces from the same animal and stimuli. Thick lines are the mean of the thin line traces. *d*, Pure-tone %  $\Delta F/F$  responses from a representative cell calculated with  $F_0$  at 1–2 s. *e*, Sound-evoked pupil responses as a percentage of average PD during the baseline epoch (gray). *f–h*, A1 principal cell response properties binned by the baseline PD at which responses occurred. Baseline PD is calculated by animal as the mean baseline PD percentage of max animal PD across the entire experiment. *f*, Mean  $\pm$  SEM of peak pure-tone %  $\Delta F/F$  responses from combined contrast conditions. *g*, Mean  $\pm$  SEM of cell reliability (trial-to-trial cross-correlation of pure-tone %  $\Delta F/F$  response). *h*, Mean  $\pm$  SEM of contrast scaling factors. *i*, The same as in *f* but with regard to contrast condition.

the intermediate range of an animal's PD [Fig. 1*f*, relative to maximum animal PD;  $p = 5.91 \times 10^{-7}$ , one-way Kruskal–Wallis test, 295 tone-responsive cells (see “2PCI processing and analysis” in Materials and Methods) from eight animals]. In further agreement with prior studies, increased trial-to-trial consistency in the timing of pure-tone responses, termed reliability, coincides with increased pure-tone response amplitudes at intermediate baseline PD (Fig. 1*g*; reliability calculated as average zero lag trial-to-trial cross-correlation between all pairs of pure-tone response  $\Delta F/F$  traces at 2–3.2 s;  $p = 3.25 \times 10^{-8}$ , one-way Kruskal–Wallis test). Thus, despite 2 s of DRC sound preceding the pure tone (Fig. 1*c*), our results are consistent with previously observed associations between baseline PD and cell pure-tone response amplitude and reliability, where intermediate baseline PD is associated with increased pure-tone amplitude and increased response reliability (McGinley et al., 2015a; Lin et al., 2019).

We next probed whether baseline PD is associated with CGC magnitude. We assessed CGC using a contrast scaling factor, defined as the population mean of individual cell average peak pure-tone responses in low contrast divided by average peak responses in high contrast (Cody and Tzounopoulos, 2022). We deemed CGC evident when contrast scaling factors were significantly  $>1$ . Contrast scaling factors plotted across baseline PD reveal that CGC is evident throughout the baseline PD range, but the magnitude of CGC is, like pure-tone response amplitudes (Fig. 1*f*), largest at intermediate baseline PDs (Fig. 1*h*;  $p = 3.03 \times 10^{-5}$ , one-way Kruskal–Wallis test). This finding suggests that baseline PD is linked to pure-tone responses that are preceded by low contrast differently from pure-tone responses that are preceded by high contrast. To further explore this contrast-dependent association between baseline PD and pure-tone responses, we plotted peak pure-tone  $\Delta F/F$  responses across baseline PD for high and low contrast (Fig. 1*i*). Consistent with Figure 1*f*, we observed a

significant association between baseline PD and response amplitude (Fig. 1*i*;  $F_{(6,1871)} = 10.74$ ,  $p = 9.04 \times 10^{-12}$ , two-way ANOVA). Notably, we found a significant interaction between contrast and baseline PD (Fig. 1*i*;  $F_{(6,1871)} = 6.01$ ,  $p = 3.10 \times 10^{-6}$ ). Thus, consistent with changing CGC magnitude along baseline PD (Fig. 1*h*), the relationship of pure-tone response amplitude to contrast is baseline PD-dependent.

### Sound-evoked PD responses are contrast-dependent but do not predict CGC magnitude

Having explored the relationship between baseline PD and CGC magnitude (Fig. 1), we next explored if evoked PD responses are contrast-dependent. Because low- and high-contrast DRC stimuli have the same average sound level, we would expect evoked PD to be comparable between contrast (Liao et al., 2016; Zekveld et al., 2018). However, sound sequences of random brief (50 ms) tone frequencies elicit larger evoked PD responses compared with sound sequences with a consistent tone frequency (Zhao et al., 2019). Thus, an alternative hypothesis is that frequency changes at sound levels farther from the mean during the high-contrast background sound would elicit larger evoked PD responses than the low-contrast DRC sound. We found that evoked PD responses to high-contrast sound are significantly larger than those in low contrast across a temporal average of the DRC stimulus (Fig. 2*a*; 0–8 s; Wilcoxon rank sum test,  $p = 0.0066$ ). To exclude any potential effect of the pure-tone stimulus, which occurs at 2 s, on evoked PD, we analyzed responses at 1–2 s and again observed significantly larger evoked PD during high contrast (Fig. 2*c*; 1–2 s; Wilcoxon rank sum test,  $p = 0.043$ ). To address the potential contribution of these neural responses in high- versus low-contrast DRCs to the observed difference in PD responses, we analyzed these neuronal responses before (CTRL, Fig. 2*d,e* top) and after ZX1 (ZX1; Fig. 2*d,e*, bottom; 520 tone-responsive cells from 14 mice). To quantify these neural

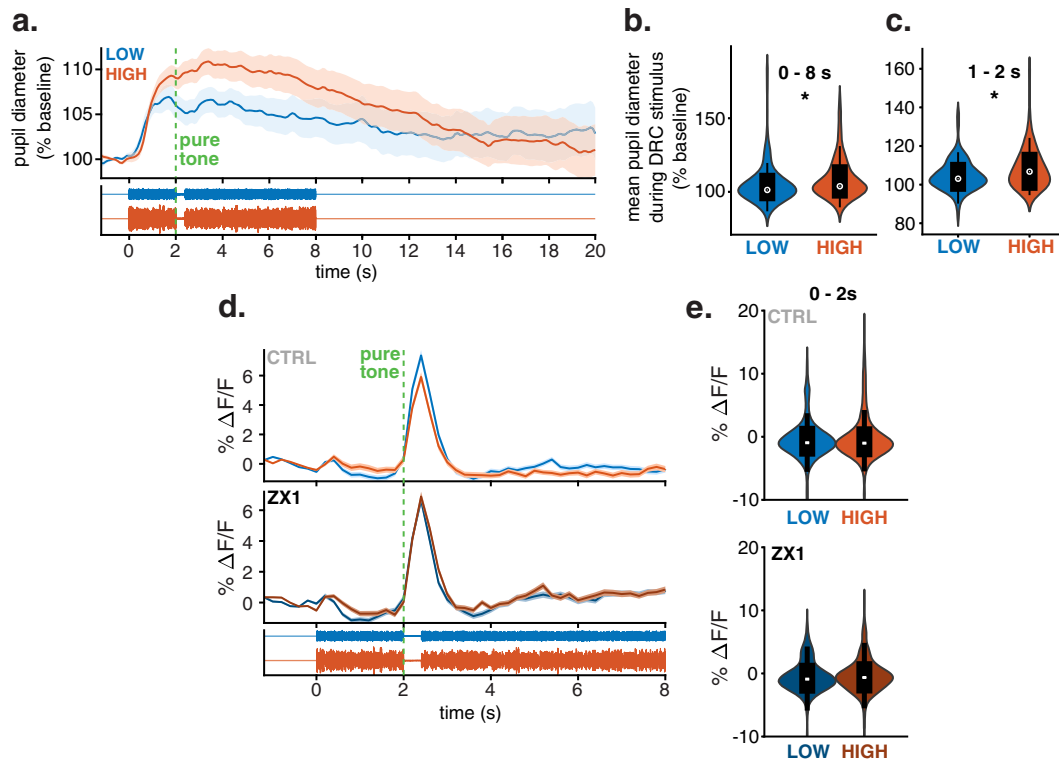


**Figure 2.** Evoked PD responses are larger in high- compared with low-contrast sound. **a**, Mean  $\pm$  SEM of contrast DRC sound-evoked pupil traces as a percentage of average baseline PD. Pure-tone (400 ms) onset denoted by the green dotted line. **b**, Violin plot of average evoked PD across the duration of DRC stimulus (0–8 s) in each contrast condition. The white dot indicates the median, the thick black line indicates the interquartile range, and the contour lines show the data distribution. **c**, The same as in **b** but across 1–2 s. The asterisk (\*) denotes  $p < 0.05$  via the Wilcoxon rank sum test. **d**, Mean  $\pm$  SEM of %  $\Delta F/F$  responses in A1 principal cells during low- (blue) and high- (orange) contrast DRC stimuli with a 400 ms pure tone occurring at 2 s (green dotted line) before (CTRL; top) and after ZX1 injection (ZX1; bottom). **e**, Violin plot of average %  $\Delta F/F$  responses in **d** across 0–2 s.

responses, we averaged cell response magnitude across 0–2 s (Fig. 2e). We did not observe any significant difference in response magnitude in either control or ZX1 (Wilcoxon rank sum test for control:  $z = 0.0073$ ,  $p = 0.9942$ ; after ZX1,  $z = -1.2425$ ,  $p = 0.2141$ ). These results suggest that the neural response magnitude to high- or low-contrast DRCs is unlikely to explain the differential evoked PDs in high versus low contrast (Fig. 2a–c).

Given this contrast dependence in the evoked PD responses, we asked whether evoked PD responses to contrast DRC predict pure-tone response amplitude and thus CGC. To evaluate this, we used a LME approach to model cell pure-tone responses as a function of baseline PD, evoked PD (average PD at 1–2 s during the DRC sound stimulus; pupil\_at\_1–2 s), and evoked PD interaction with sound contrast (Fig. 3; see “Pupillometry: analysis” in Materials and Methods for a description of the full model). We analyzed the contribution of these input factors using a coefficient test to determine whether they significantly contribute to predicting neuronal pure-tone responses (Fig. 3b). Consistent with the observed association between baseline PD and pure-tone responses (Fig. 1f), we found that the baseline PD model coefficient significantly differed from zero and thus significantly contributed to neuronal responses ( $F_{(1,165.06)} = 8.70$ ;  $p = 3.64 \times 10^{-3}$ ). Neither sound-evoked PD responses ( $F_{(1,167.17)} = 2.61$ ;  $p = 0.108$ ) nor their interaction with contrast ( $F_{(1,169.59)} = 0.0971$ ;  $p = 0.756$ ) contributed to predicting neuronal pure-tone responses. To further validate this, we used a likelihood ratio test to compare the full LME model with a null model that solely includes baseline PD as a predictor (Fig. 3c; see “Pupillometry: analysis” in Materials and Methods for a description of the null model). The full model including

sound-evoked PD responses and their interaction with contrast did not significantly improve neuronal pure-tone response prediction when compared with the null model ( $p = 0.330$ ). Thus, although evoked PD responses are contrast-dependent, these results are consistent with the notion that evoked PD does not contribute to adaptation to sound contrast in A1 (CGC).

### Cortical synaptic zinc signaling is necessary for the increased evoked PD in high- versus low-contrast sound

As our results suggest that sound contrast-dependent evoked PD responses do not contribute to neuronal adaptation to contrast in A1 (CGC; Fig. 3), we next assessed whether CGC in A1 or more specifically, its associated cortical neuromodulatory signaling contributes to contrast-dependent evoked PD responses. We recently established that either genetic or chemical disruption of cortical zinc signaling eliminated A1 sound CGC in mice (Cody and Tzounopoulos, 2022). Therefore, we probed whether cortical synaptic zinc signaling is needed for the contrast dependence of evoked PD responses. Namely, we injected ZX1, an extracellular high-affinity zinc-specific chelator (Pan et al., 2011; Anderson et al., 2015), into the ACTx of WT mice (ZnT3-WT; Fig. 4a) and knock-out mice (ZnT3-KO; Fig. 4b) that lack ZnT3 and thus synaptic zinc (Cole et al., 1999). We analyzed neuronal responses before (CTRL) and after ZX1 (ZX1). To quantify the effect of contrast and ZX1 on evoked PD, we fit a LME model using GCA (Fig. 4c,d; Mirman, 2016; Montes-Lourido et al., 2021). In ZnT3-WT mice, we observed a significant effect of both contrast and ZX1 on the intercept, which represents the entire temporal response average, and on the first-order (linear) time polynomial coefficient (slope), which

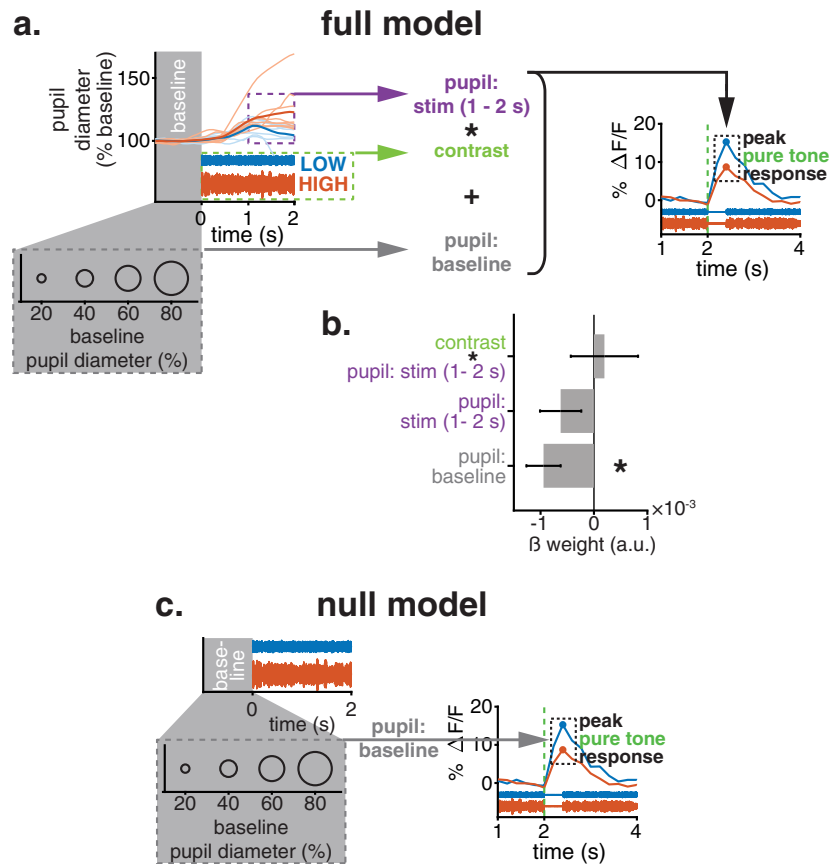


**Figure 3.** Contrast-dependent changes in evoked PD do not contribute to CGC. **a**, Depiction of full LME model input factors (left) for assessing contribution to the prediction of cell peak pure-tone response output (right; same representative cell as in Fig. 1). **b**, Coefficient weights of full model factors depicted in **a**. **c**, Depiction of null LME model consisting solely of baseline pupil size factor for comparison to the full model via likelihood ratio test.

represents the PD rate of change (Fig. 4c; contrast intercept,  $F_{(1,7921.6)} = 19.48$ ,  $p = 1.03 \times 10^{-5}$ ; contrast slope,  $F_{(1,7918.8)} = 26.54$ ,  $p = 2.64 \times 10^{-7}$ ; ZX1 intercept,  $F_{(1,7926.3)} = 4.47$ ,  $p = 0.0344$ ; ZX1 slope,  $F_{(1,7918.8)} = 40.45$ ,  $p = 2.13 \times 10^{-10}$ ). We also observed a significant interaction between contrast and ZX1 treatment (Fig. 4c,  $F_{(1,7921.6)} = 24.2$ ,  $p = 8.85 \times 10^{-7}$ ). Pairwise post hoc Tukey tests revealed a significant effect of contrast before, but not after ZX1 treatment, and solely a significant effect of ZX1 on high-contrast-evoked PD ( $p < 0.0001$  for both comparisons). Notably, the high-contrast-specific effect of ZX1 on evoked PD mirrors the high-contrast-specific effect of ZX1 on A1 PN responses (Cody and Tzounopoulos, 2022). This similarity is consistent with a link between A1 CGC and contrast-dependent effects on evoked PD responses; however, our results do not prove this relationship directly (see Discussion). Nonetheless, these results support that cortical zinc signaling is necessary for contrast-dependent increases in evoked PD during high- versus low-contrast sound.

In ZnT3-KO mice (Fig. 4b), we did not observe a significant effect of either contrast or ZX1 on evoked PD intercept (Fig. 4d,f; contrast,  $F_{(1,4500.8)} = -1.14$ ,  $p = 0.255$ ; ZX1,  $F_{(1,4502.4)} = 1.45$ ,  $p = 0.147$ ), nor a significant interaction between the two ( $F_{(1,4500.2)} = -0.540$ ,  $p = 0.589$ ). Thus, the effect of contrast on pupil responses is ZnT3-dependent. In ZnT3-KO mice, we did not observe a significant effect of contrast on the evoked PD slope (Fig. 4f;  $F_{(1,4500.0)} = 1.31$ ,  $p = 0.190$ ); however, we observed a significant effect of ZX1 ( $F_{(1,4500.0)} = -2.49$ ,  $p = 0.0129$ ). The lack of an interaction between contrast and ZX1 suggests a

ZnT3-independent but zinc-dependent effect on slope. However, this ZnT3-independent effect is small, as the GCA slope coefficient (weight) for ZX1 in the ZnT3-KO mice ( $-0.64$ , Fig. 4f) was less than half that of ZnT3-WT ( $-1.41$ , Fig. 4e). Taken together, these results reveal that cortical synaptic zinc signaling is necessary for increases in evoked PD during high- versus low-contrast sound.

To better understand how a unilateral ACTx manipulation (ZX1 infusion) can affect evoked PD responses, which presumably reflect more general processes and brain areas related to arousal, we explored the contra- and ipsilateral effects of unilateral ZX1 injection in ACTx. Namely, we tested the effect of contralateral ZX1 infusion on responses to sound in ACTx ipsilateral to imaging (Fig. 5). Our previous studies have shown that chelation of ipsilateral ACTx zinc with ZX1 infusion reduced sound-evoked responses of principal L2/3 ACTx neurons imaged in the ipsilateral A1 (Kumar et al., 2019). Here, to test whether ZX1 infusion affects the sound-evoked responses of contralateral A1 and whether ZX1 travels to other hemisphere, we performed in vivo WF imaging of right (ipsilateral) A1 PNs expressing GCaMP6f, before and after infusion of ZX1 + Alexa Fluor 594 (red dye) to contralateral (left) ACTx (Fig. 5a,b). To infuse ZX1 into contralateral ACTx, we implanted chronic cannulas to the left ACTx, as described previously (Kumar et al., 2019) and illustrated in Figure 5a. We found that the infusion of ZX1 + Alexa Fluor 594 to the left (contralateral) ACTx does not show the presence of Alexa Fluor 594 in the ipsilateral ACTx under the red channel (Fig. 5c), suggesting that ZX1 does not travel to the other

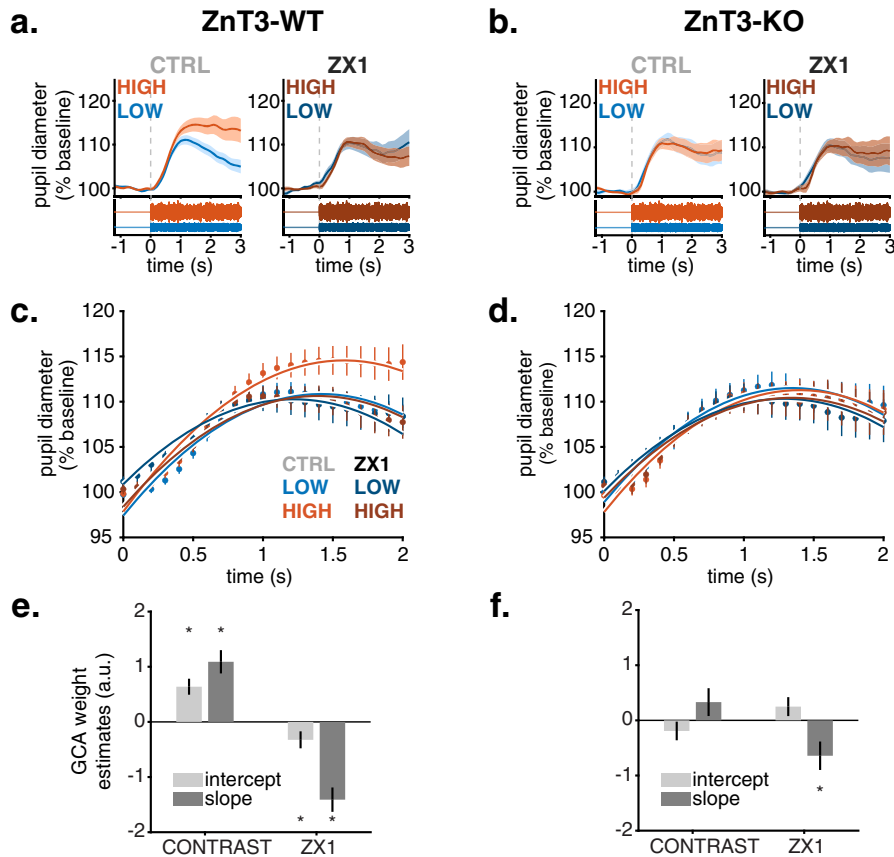


**Figure 4.** Cortical synaptic zinc signaling is necessary for contrast-dependent changes in evoked PD responses. *a*, ZnT3-WT mice: mean  $\pm$  SEM of sound-evoked pupil responses to low- (blue) and high- (orange) contrast DRC stimuli without a pure tone at 2 s. Responses shown before (left, CTRL) and after injection of ZX1 (right, ZX1) into the auditory cortex of ZnT3-WT mice. *b*, The same as in *a* but in ZnT3-KO mice. *c*, ZnT3-WT mice: same responses as in *a* limited to 0–2 s into DRC onset with fitted polynomials from GCA. *d*, same as in *c* but in ZnT3-KO mice. *e*, ZnT3-WT mice: GCA model weight estimates of fitted responses in *c* for contrast and ZX1 model factors (LME model intercept and first-order orthogonal polynomial coefficient, slope). *f*, The same as in *e* but in ZnT3-KO mice.

cortical hemisphere (see Discussion). Importantly, we found that infusion of ZX1 to the contralateral ACTx increased the sound-evoked responses of ipsilateral A1 PN (Fig. 5*c–e*; three mice, one-way repeated measure ANOVA,  $F = 33.44$ ,  $p = 4.1 \times 10^{-5}$ ; control vs ZX1 in contralateral ACTx,  $p = 0.016$ , Bonferroni's multiple-comparisons test), suggesting that ZX1 affects the sound-evoked responses of A1 neurons that are located contralaterally to the ZX1 injection. Furthermore, consistent with previous results (Anderson et al., 2017), subsequent infusion of ZX1 to ipsilateral ACTx reduced the sound-evoked responses of A1 PN (Fig. 5*d–f*; ZX1 in contralateral vs ipsilateral ACTx,  $p = 3.2 \times 10^{-5}$ , Bonferroni's multiple-comparisons test). Overall, these results show that a unilateral ACTx ZX1 injection can still impact contralateral ACTx, despite ZX1 diffusion being limited to the injected hemisphere. Thus, such contralateral effects may not be excluded as a potential contribution to observed ZX1 effects on evoked PD responses (see Discussion).

We observed a significant time-dependent increase in baseline PD across the recording duration of ZX1 experiments [Fig. 6*a*; slope 95% CI = (0.0798, 0.183),  $p = 1.26 \times 10^{-6}$ ]. Given that the pupil tends to constrict at relatively dilated states (de Gee et al., 2014; Mridha et al., 2021), this could pose a problem in the interpretation of our results. To control for this, we used ACSF as a control and found a similar time-dependent increase in baseline PD [Fig. 6*a*; slope 95% CI = (0.0159, 0.279),  $p = 0.0282$ ]. Thus, in both ZX1 and ACSF, we observed a nonspecific, time-dependent

increase in PD. However, the 95% CIs for the two conditions overlap, suggesting that this effect is not different between ZX1 and ACSF. Importantly, following ACSF injection, unlike following ZX1 injection (Fig. 4*a,c,e*), we observed a significant effect of contrast on both the intercept and fitted slope coefficient of the first-order time polynomial (Fig. 6*b*; intercept,  $F_{(1,2558.3)} = 46.22$ ,  $p = 1.31 \times 10^{-11}$ ; slope,  $F_{(1,2558)} = 15.076$ ,  $p = 1.10 \times 10^{-4}$ ), which means that the difference in PD in high versus low contrast is still evident after the ACSF treatment, which is matched in time and mode of application with the ZX1 treatment. This result further supports that the effects of ZX1 on evoked PD are not due to the time-dependent increase in baseline PD. Moreover, we limited our pupil response analyses to the 50th percentile of baseline PD (see “Pupillometry: analysis” in Materials and Methods) at which there was no significant correlation between baseline PD and evoked PD (Fig. 6*c*; Pearson's correlation coefficient,  $r_{(238)} = -0.0928$ ,  $p = 0.1537$ ). Together, these results suggest that the effect of ZX1 on eliminating contrast-dependent increases in evoked PD during high- versus low-contrast sound is not due to either the injection of a solution volume into ACTx or to potential non-zinc-specific effects of ZX1 on baseline PD throughout the experiment; the effect of ZX1 are specific to zinc chelation.

As an additional control for potential effects of the recording duration or potential ZX1 confounds, we used a LME GCA model to compare PD responses in high contrast between ZnT3-WT and ZnT3-KO mice prior to ZX1 injection. We



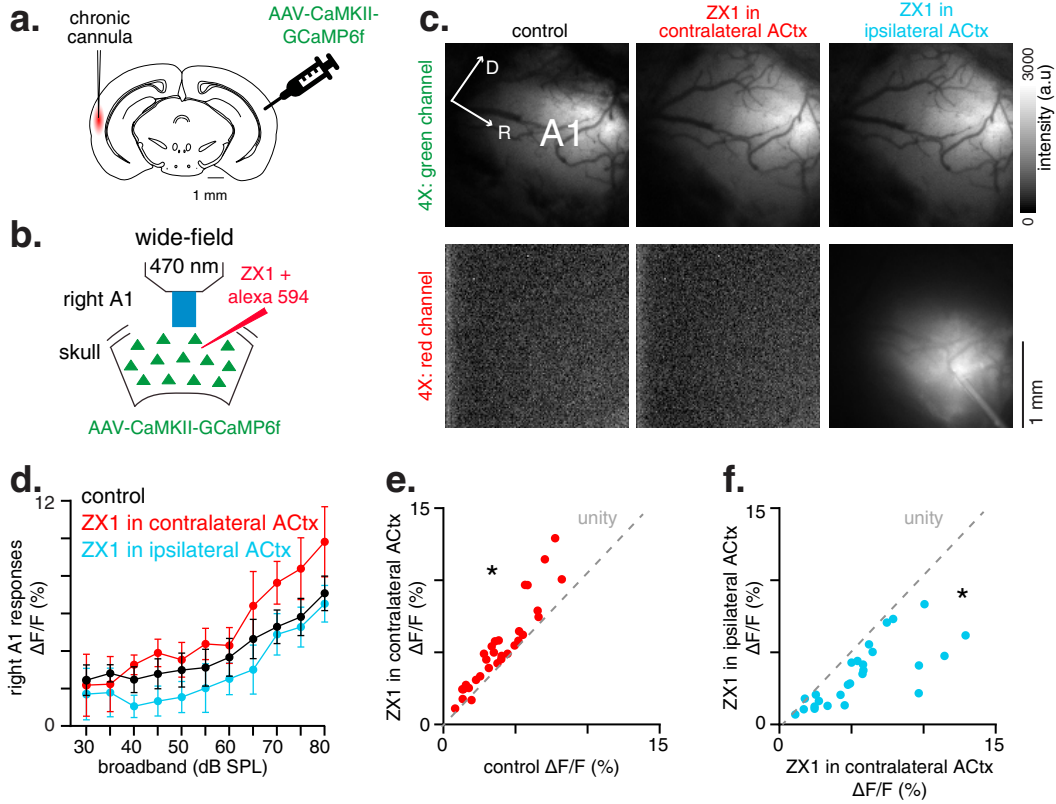


**Figure 5.** Unilateral infusion and diffusion of ZX1 affect neuronal sound responses in both auditory cortical hemispheres. **a**, Schematic illustration of chronic cannula implantation in the left (contralateral) ACtx and AAV9-CaMKIIII-GCaMP6f injection in the right (ipsilateral) ACtx in mice. **b**, WF imaging experimental design for A1 PNs in the ipsilateral cortical hemisphere. **c**, Representative images showing expression of GCaMP6f via the green channel and presence of ZX1 and Alexa Fluor 594 (red dye) via the red channel. **d**, Black: average sound-evoked responses of ipsilateral A1 PNs to broadband sounds (6–64 kHz, 100 ms long) in control conditions. Red: average sound-evoked responses of ipsilateral A1 PNs after infusion of ZX1 in the contralateral ACtx. Cyan: average sound-evoked responses of ipsilateral A1 PNs after infusion of ZX1 in ipsilateral ACtx. **e**, Scatter plots showing sound-evoked responses of the ipsilateral A1 PNs before (control) versus sound-evoked responses of the ipsilateral A1 after ZX1 infusion in contralateral ACtx. **f**, Scatter plots showing sound-evoked responses of the ipsilateral A1 PNs after infusion of ZX1 in contralateral ACtx versus sound-evoked responses of the ipsilateral A1 PNs after infusion of ZX1 in the ipsilateral ACtx.

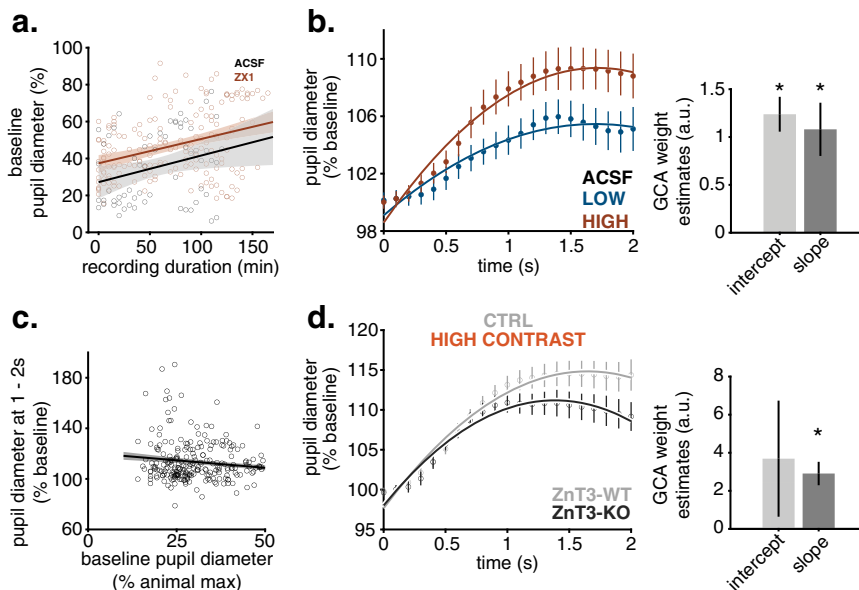


**Figure 6.** Cortical synaptic zinc signaling is necessary for increases in evoked PD in high-contrast sound. **a**, Open circles: mean baseline PD plotted against experiment recording duration during ACSF (black) and ZX1 (orange) experiments. Black and orange lines with shading: fitted ACSF and ZX1 (respectively) regression lines and 95% CI. **b**, Left: mean  $\pm$  SEM of sound-evoked pupil responses to low- (blue) and high- (orange) contrast DRC stimuli after ACSF injection with fitted GCA polynomials. **b**, Right: GCA model weight estimates. **c**, Open circles: mean of evoked pupil responses 1–2 s into DRC stimulus across both contrast conditions plotted against the baseline PD that preceded them. Black line: fitted regression line with gray 95% CI. **d**, Left: evoked PD increases in high-contrast sound before ZX1 injection (CTRL) from ZnT3-WT (gray) and ZnT3-KO (black) mice with fitted GCA polynomials (Fig. 4a,b, light orange–shaded responses). **d**, Right: GCA model weight estimates.

observed a significant effect of genotype on the slope coefficient of the first-order time polynomial (Fig. 6*d*;  $F_{(1,3869)} = 22.37$ ,  $p = 2.33 \times 10^{-6}$ ). Namely, ZnT3-KO mice have reduced PD responses in high contrast, consistent with the high-contrast-dependent effect of synaptic zinc signaling on evoked PD. Taken together, these results demonstrate that cortical synaptic zinc signaling is necessary for increases in evoked PD in high-versus low-contrast sound.

## Discussion

To study the contribution of baseline PD to sensory processing and adaptation, we paired pupillometry with a two-photon imaging assay of sound CGC in ACtx. Our results support that CGC is strongest at an intermediate baseline PD range where sound responses are maximal. We then disrupted cortical synaptic zinc signaling, which is necessary for CGC, and used the same preparation to explore the relationship between neuromodulation in the sensory cortex and evoked PD changes (Cody and Tzounopoulos, 2022). Our data suggest that cortical neuromodulatory synaptic zinc signaling is necessary for increases in PD in response to high-contrast sound compared with low-contrast sound.

PD changes have been linked to neuromodulatory systems in previous studies (Joshi and Gold, 2020; Joshi, 2021). Recordings of acetylcholine (ACh) and norepinephrine (NE) projections in layer 1 of the mouse cortex during pupillometry reveal that both ACh and NE correlate with PD, albeit on different time scales, and that both pupil and projection activity increases prior to locomotion onset (Reimer et al., 2016). Furthermore, vagus nerve stimulation, which is associated with both cortical ACh release and LC-NE activation, drives pupil dilation (Mridha et al., 2021). Finally, a serotonin-dependent link between PD and task-related uncertainty has been recently discovered, whereby the level of the effect of serotonergic neuronal activation on PD depends on task-related uncertainty (Cazettes et al., 2020). By revealing that contrast-dependent changes in evoked PD require cortical neuromodulatory zinc signaling, our results broaden our understanding of the relationship between neuromodulatory systems and changes in PD. Because we demonstrated this dependence without the use of any artificial stimulation of zincergic signaling, we propose that contrast-dependent changes in PD provide a physiological readout of zincergic neuromodulatory synaptic zinc activity in the sensory cortex.

Our observed baseline PD effects on CGC are consistent with a baseline PD-indexed cortical state that interacts with sound contrast and persists for at least 2 s. This interaction cannot easily be explained by momentary fluctuations in membrane potential during brief (~1–2 s) baseline pupil dilations (Reimer et al., 2014; McGinley et al., 2015a) because baseline PD is measured across a 4 s average and CGC is measured 2 s after that. Animal movement effects (Vinck et al., 2015) are also an unlikely factor to explain this interaction, because the PD range at which we observe increasing CGC (Fig. 1*h*; ~20–50% animal PD max) is well below the PD range associated with locomotion (>70% animal PD max; McGinley et al., 2015a,b). In agreement with an interaction between sound contrast and baseline PD, solely at the intermediate baseline PD range where CGC is maximal, we observed a significant effect of contrast on pure-tone responses between low and high contrast ( $p = 3.65 \times 10^{-5}$ , Bonferroni's corrected post hoc test): compare Figure 1*h* at baseline PD of 43–54%, fourth data point from the left, with the same baseline point at PD range in Figure 1*i*. However, because the contrast scaling

factor is above 1 at each baseline PD range (Fig. 1*h*), the high-contrast responses in Figure 1*i* would be expected to be lower than the low-contrast responses at all baseline PD ranges in Figure 1*i*. The contrast scaling factor measure of CGC (Fig. 1*h*) is calculated from each cell's average peak response in low contrast divided by its peak response in high contrast, whereas responses in Figure 1*i* are not paired ratios by cell. The discrepancy between Figure 1*h* and 1*i* may thus be explained by response variability among cells. Taken together, at intermediate baseline PD, contrast effects are evident across average cell population responses, rather than being limited to effects relative to each cell.

Do contrast-dependent changes in evoked PD relate to baseline PD-indexed cortical state? Cortical membrane potential variability strongly correlates with baseline PD (Reimer et al., 2014; McGinley et al., 2015a); however, changes in sound contrast alone do not affect cortical membrane potential variability (Cooke et al., 2020). Moreover, cortical CGC magnitude depends on baseline PD (Fig. 1*h*), but contrast-evoked PD does not predict CGC (Fig. 3). Together, these findings suggest that contrast-dependent changes in evoked PD are reflective of cortical activity that is different from the activity that is indexed by baseline PD. Furthermore, increases in evoked PD are associated with increased neural gain (firing-rate scaling; Schwartz et al., 2019). Our results suggest that PD has an opposite relationship with gain that is modeled by a change in the slope of the sigmoidal neural response function that reflects CGC. Gain is decreased during high- versus low-contrast sound (Rabinowitz et al., 2011; Lohse et al., 2020; Cody and Tzounopoulos, 2022), yet we observed increased evoked PD during high versus low contrast. Thus, our results suggest a previously unknown relationship between cortical state and evoked PD changes. Indeed, our studies reveal a hierarchical scheme whereby cortical synaptic zinc signals a cortical state that is, in turn, necessary for increased evoked PD.

Numerous sound stimulus factors influence evoked PD, such as loudness, deviance from regularity, complexity, and signal-to-noise to name a few (Wang et al., 2014; Liao et al., 2016; Zekveld et al., 2018; Zhao et al., 2019; Montes-Lourido et al., 2021). Yet, it is unclear which stages of the ascending auditory pathway contribute to these differences in evoked PD or to changes in cognitive states that in turn affect PD. Inversely, when sound-evoked PD responses are compared with healthy human subjects, differences in evoked PD are indicative of altered neurophysiology and sensory processing associated with hearing loss, dementia, and schizophrenia (Zekveld et al., 2018). Because our results support that increases in evoked PD in high- versus low-contrast sound is a marker for intact cortical zinc signaling, and, likely for intact CGC (see the last paragraph in Discussion), we propose that PD may thus serve as a basis for a pupillometry marker of impaired cortical neuromodulation.

Our pharmacological perturbation of zinc signaling (via ZX1) is limited to the sensory cortex. This is consistent with the reported intracortical diffusion area of ZX1,  $2.1 \pm 0.1 \text{ mm}^2$ , based on the spread of ZX1 coinjected with Alexa Fluor 594 (Anderson et al., 2017). As noted in Cody and Tzounopoulos (2022), if converted to the radius ( $0.8 \pm 0.2 \text{ mm}$ ), this suggests that the spread of ZX1 is limited exclusively to the cortex (Lein et al., 2007). Thus, we propose that sound contrast-dependent effects on evoked PD responses are ACtx-dependent. We delivered sound stimuli to the left ear, injected ZX1 unilaterally into the right ACtx, and recorded ipsilateral (right) pupil and ACtx responses. Pupil responses to sound stimuli persisted with both

pharmacological and transgenic blockade of zinc signaling, but, upon blockade, responses to both low and high contrast resembled low-contrast responses, which were of comparable magnitude in ZnT3-WT and ZnT3-KO mice (Fig. 4).

Although ZX1 diffusion was likely limited to the injected hemisphere (Fig. 5c), we observed ZX1-dependent effects on neural responses to sound stimuli in ACTx contralateral to injection (Fig. 5c–e). Thus, despite the unilateral ZX1 infusion and diffusion, the observed effects of zinc signaling on sound-evoked PD responses (Fig. 4) may arise from ZX1-dependent effects on the sound-evoked responses of A1 neurons that are located contralaterally to the ZX1 injection. Consistent with a bilateral ZX1 effect, the magnitude of PD responses to high-contrast sound after ZX1 infusion in ZnT3-WT mice (Fig. 4c; peak at ~110% PD) is not different from the magnitude of high-contrast PD responses in ZnT3-KO mice (Fig. 4d; peak at ~110% PD), which lack ZnT3 bilaterally. The effect of ZX1 injection contralaterally to the imaged cortical hemisphere may involve a circuit effect mediated by L2/3 corticocortical (IT) neurons, which are zincergic and project to the contralateral hemisphere (Kouvaros et al., 2023). The effect of zinc signaling in PD is unlikely to be mediated by either somatostatin- (SOM) or parvalbumin-expressing (PV) neurons, as zinc signaling does not have any sound contrast-dependent effects on either PV or SOM neurons (Cody and Tzounopoulos, 2022). However, an indirect network effect including both interneurons and IT neurons cannot be excluded. Nonetheless, responses to sound in the hemisphere contralateral to ZX1 infusion, regardless of how affected they are by the physical occlusion via the acute surgical preparation (see “Acute surgery preparation for in vivo imaging” in Materials and Methods), could still be impacted by ipsilateral ZX1 infusion and thereby influence sound-evoked PD responses.

Although we have not addressed this question in this manuscript, a pathway from ACTx to pupil could occur via ascending projections to the prefrontal cortex (PFC; Romanski et al., 1999) and/or descending projections to the superior colliculus (SC; Zingg et al., 2017). The PFC connections would then reach the pupil via the LC, which projects to the Edinger–Westphal nucleus (EWN), which in turn innervates neurons controlling the muscles of the pupil (Joshi and Gold, 2020). As pupil dilation mediated by the LC is lateralized (Liu et al., 2017), a systematic laterality in the difference between low- and high-contrast-evoked PD would support that the effect of contrast on the pupil is mediated by LC. ACTx connections to the pupil via SC would occur via a direct path from the SC to EWN (Joshi and Gold, 2020). Further studies are needed to address the underlying circuitry. Nonetheless, the influence of cortical zinc signaling on contrast-dependent-evoked PD responses suggests a role of zinc signaling in the long-range coordination of neural activity for multisensory processing.

Although we did not address whether it is the computation of cortical CGC that triggers contrast-dependent changes in evoked PD, it is an attractive hypothesis. Cortical zinc signaling is necessary for both CGC and contrast-dependent increases in evoked PD (Cody and Tzounopoulos, 2022). In both cases, cortical zinc signaling decreases the amplitude of both neuronal and PD responses specifically in high contrast, while leaving these parameters unaffected in low contrast. CGC is achieved via a canonical neural computation, normalization (Carandini and Heeger, 2012), which is conserved among species (Rabinowitz et al., 2011; Cooke et al., 2018; Lohse et al., 2020) and sensory domains (Schwartz and Simoncelli, 2001; Olsen et al., 2010; Carandini and Heeger, 2012; Wilson et al., 2012; Lohse et al.,

2020). Moreover, CGC accounts for changes in perceptual judgments in humans and mice (Lohse et al., 2020; Angeloni et al., 2021) and thus contributes to a conserved universal perceptual phenomenon that does not require any training. Although not tested in this manuscript, one tempting hypothesis is that evoked PD changes between low and high sound contrast are reflective of sensory processing changes that might be the result of a universal and evolutionarily conserved “internalization” of ethologically relevant changes in natural sound statistics into cortical circuits. In this context, we propose that our results may provide a cortical neuromodulatory mechanism that conveys a specific pupil-indexed change in sensory processing state from low- to high-contrast sound contexts. In this way, ethologically relevant changes in stimulus statistics likely initiate changes in pupil-indexed arousal and multisensory processing that are evident in other organisms via changes in PD. As such, these studies hold the potential to add fundamental insight into how the brain can efficiently handle the universals of the external world delivered via sensory inputs. Together, these studies may provide a new physiological structure in the internal functional brain space that transforms sensory input into motor output.

## References

- Anderson CT, Radford RJ, Zastrow ML, Zhang DY, Apfel U-P, Lippard SJ, Tzounopoulos T (2015) Modulation of extrasynaptic NMDA receptors by synaptic and tonic zinc. *Proc Natl Acad Sci U S A* 112:E2705–E2714.
- Anderson CT, Kumar M, Xiong S, Tzounopoulos T (2017) Cell-specific gain modulation by synaptically released zinc in cortical circuits of audition. *Elife* 6:e29893.
- Angeloni CF, Mlynarski W, Piasini E, Williams AM, Wood KC, Garami L, Hermundstad A, Geffen MN (2021) Cortical efficient coding dynamics shape behavioral performance. *bioRxiv:2021.08.11.455845*.
- Bender PTR, McCollum M, Boyd-Pratt H, Mendelson BZ, Anderson CT (2023) Synaptic zinc potentiates AMPA receptor function in mouse auditory cortex. *Cell Rep* 42:112932.
- Brown CE, Dyck RH (2002) Rapid, experience-dependent changes in levels of synaptic zinc in primary somatosensory cortex of the adult mouse. *J Neurosci* 22:2617–2625.
- Carandini M, Heeger DJ (2012) Normalization as a canonical neural computation. *Nat Rev Neurosci* 13:51–62.
- Cazettes F, Reato D, Morais JP, Renart A, Mainen ZF (2020) Phasic activation of dorsal raphe serotonergic neurons increases pupil size. *Curr Biol* 31:192–197.e4.
- Chen Q, et al. (2020) Dysfunction of cortical GABAergic neurons leads to sensory hyper-reactivity in a Shank3 mouse model of ASD. *Nat Neurosci* 23:520–532.
- Cody PA, Tzounopoulos T (2022) Neuromodulatory mechanisms underlying contrast gain control in mouse auditory cortex. *J Neurosci* 42:5564–5579.
- Cole TB, Wenzel HJ, Kafer KE, Schwartzkroin PA, Palmiter RD (1999) Elimination of zinc from synaptic vesicles in the intact mouse brain by disruption of the ZnT3 gene. *Proc Natl Acad Sci U S A* 96:1716–1721.
- Cooke JE, King AJ, Willmore BDB, Schnupp JWH (2018) Contrast gain control in mouse auditory cortex. *J Neurophysiol* 120:1872–1884.
- Cooke JE, Kahn MC, Mann EO, King AJ, Schnupp JWH, Willmore BDB (2020) Contrast gain control occurs independently of both parvalbumin-positive interneuron activity and shunting inhibition in auditory cortex. *J Neurophysiol* 123:1536–1551.
- de Gee JW, Knapen T, Donner TH (2014) Decision-related pupil dilation reflects upcoming choice and individual bias. *Proc Natl Acad Sci U S A* 111:E618–E625.
- Dyck RH, Chaudhuri A, Cynader MS (2003) Experience-dependent regulation of the zincergic innervation of visual cortex in adult monkeys. *Cereb Cortex* 13:1094–1109.
- Joshi S (2021) Pupillometry: arousal state or state of mind? *Curr Biol* 31:R32–R34.
- Joshi S, Gold JI (2020) Pupil size as a window on neural substrates of cognition. *Trends Cogn Sci* 24:466–480.

- Joshi S, Li Y, Kalwani RM, Gold JI (2016) Relationships between pupil diameter and neuronal activity in the locus coeruleus, colliculi, and cingulate cortex. *Neuron* 89:221–234.
- Keemink SW, Lowe SC, Pakan JMP, Dylida E, van Rossum MCW, Rochefort NL (2018) FISSA: a neuropil decontamination toolbox for calcium imaging signals. *Sci Rep* 8:3493.
- Kerlin AM, Andermann ML, Berezovskii VK, Reid RC (2010) Broadly tuned response properties of diverse inhibitory neuron subtypes in mouse visual Cortex. *Neuron* 67:858–871.
- Kouvaros S, Kumar M, Tzounopoulos T (2020) Synaptic zinc enhances inhibition mediated by somatostatin, but not parvalbumin, cells in mouse auditory cortex. *Cereb Cortex* 30:3895–3909.
- Kouvaros S, Bizup B, Solis O, Kumar M, Ventriglia E, Curry FP, Michaelides M, Tzounopoulos T (2023) A CRE/DRE dual recombinase transgenic mouse reveals synaptic zinc-mediated thalamocortical neuromodulation. *Sci Adv* 9:eadf3525.
- Krall RF, Moutal A, Phillips MB, Asraf H, Johnson JW, Khanna R, Hershfinkel M, Aizenman E, Tzounopoulos T (2020) Synaptic zinc inhibition of NMDA receptors depends on the association of GluN2A with the zinc transporter ZnT1. *Sci Adv* 6:eabb1515.
- Kumar M, Xiong S, Tzounopoulos T, Anderson CT (2019) Fine control of sound frequency tuning and frequency discrimination acuity by synaptic zinc signaling in mouse auditory cortex. *J Neurosci* 39:854–865.
- Larson MD, Behrends M (2015) Portable infrared pupillometry: a review. *Anesth Analg* 120:1242–1253.
- Lein ES, et al. (2007) Genome-wide atlas of gene expression in the adult mouse brain. *Nature* 445:168–176.
- Liao H-I, Kidani S, Yoneya M, Kashino M, Furukawa S (2016) Correspondences among pupillary dilation response, subjective salience of sounds, and loudness. *Psychon Bull Rev* 23:412–425.
- Lin P-A, Asinof SK, Edwards NJ, Isaacson JS (2019) Arousal regulates frequency tuning in primary auditory cortex. *Proc Natl Acad Sci U S A* 116:25304–25310.
- Linden JF, Liu RC, Sahani M, Schreiner CE, Merzenich MM (2003) Spectrotemporal structure of receptive fields in areas AI and AAF of mouse auditory cortex. *J Neurophysiol* 90:2660–2675.
- Liu Y, Rodenkirch C, Moskowitz N, Schriver B, Wang Q (2017) Dynamic lateralization of pupil dilation evoked by locus coeruleus activation results from sympathetic, not parasympathetic, contributions. *Cell Rep* 20:3099–3112.
- Lohse M, Bajo VM, King AJ, Willmore BDB (2020) Neural circuits underlying auditory contrast gain control and their perceptual implications. *Nat Commun* 11:324.
- Mathis A, Mamidanna P, Cury KM, Abe T, Murthy VN, Mathis MW, Bethge M (2018) DeepLabCut: markerless pose estimation of user-defined body parts with deep learning. *Nat Neurosci* 21:1281–1289.
- McAllister BB, Dyck RH (2017) Sound processing: a new role for zinc in the brain. *Elife* 6:e31816.
- McGinley MJ, David SV, McCormick DA (2015a) Cortical membrane potential signature of optimal states for sensory signal detection. *Neuron* 87:179–192.
- McGinley MJ, Vinck M, Reimer J, Batista-Brito R, Zgha E, Cadwell CR, Tolias AS, Cardin JA, McCormick DA (2015b) Waking state: rapid variations modulate neural and behavioral responses. *Neuron* 87:1143–1161.
- Mirman D (2016) *Growth curve analysis and visualization using R*. Boca Raton: Chapman and Hall/CRC.
- Montes-Lourido P, Kar M, Kumbam I, Sadagopan S (2021) Pupillometry as a reliable metric of auditory detection and discrimination across diverse stimulus paradigms in animal models. *Sci Rep* 11:3108.
- Morabito A, Zerlaut Y, Serraz B, Sala R, Paoletti P, Rebola N (2022) Activity-dependent modulation of NMDA receptors by endogenous zinc shapes dendritic function in cortical neurons. *Cell Rep* 38:110415.
- Mridha Z, de Gee JW, Shi Y, Alkashgari R, Williams J, Suminski A, Ward MP, Zhang W, McGinley MJ (2021) Graded recruitment of pupil-linked neuromodulation by parametric stimulation of the vagus nerve. *Nat Commun* 12:1539.
- Nath T, Mathis A, Chen AC, Patel A, Bethge M, Mathis MW (2019) Using DeepLabCut for 3D markerless pose estimation across species and behaviors. *Nat Protoc* 14:2152–2176.
- Olsen SR, Bhandawat V, Wilson RI (2010) Divisive normalization in olfactory population codes. *Neuron* 66:287–299.
- Pan E, Zhang X, Huang X, Krezel A, Zhao M, Tinberg CE, Lippard SJ, McNamara JO (2011) Vesicular zinc promotes presynaptic and inhibits postsynaptic long-term potentiation of mossy fiber-CA3 synapse. *Neuron* 71:1116–1126.
- Paoletti P, Vergnano AM, Barbour B, Casado M (2009) Zinc at glutamatergic synapses. *Neuroscience* 158:126–136.
- Pinheiro JC, Bates DM (2000) Extending the basic linear mixed-effects model. In: *Mixed-effects models in S and S-PLUS*, pp 201–270 *statistics and computing* (Pinheiro JC, Bates DM, eds). New York, NY: Springer.
- Pnevmatikakis EA, Giovannucci A (2017) NoRMCorre: an online algorithm for piecewise rigid motion correction of calcium imaging data. *J Neurosci Methods* 291:83–94.
- Privitera M, et al. (2020) A complete pupillometry toolbox for real-time monitoring of locus coeruleus activity in rodents. *Nat Protoc* 15:2301–2320.
- Rabinowitz NC, Willmore BDB, Schnupp JWH, King AJ (2011) Contrast gain control in auditory cortex. *Neuron* 70:1178–1191.
- Reimer J, Froudarakis E, Cadwell CR, Yatsenko D, Denfield GH, Tolias AS (2014) Pupil fluctuations track fast switching of cortical states during quiet wakefulness. *Neuron* 84:355–362.
- Reimer J, McGinley MJ, Liu Y, Rodenkirch C, Wang Q, McCormick DA, Tolias AS (2016) Pupil fluctuations track rapid changes in adrenergic and cholinergic activity in cortex. *Nat Commun* 7:13289.
- Romanski LM, Tian B, Fritz J, Mishkin M, Goldman-Rakic PS, Rauschecker JP (1999) Dual streams of auditory afferents target multiple domains in the primate prefrontal cortex. *Nat Neurosci* 2:1131–1136.
- Romero S, Hight AE, Clayton KK, Resnik J, Williamson RS, Hancock KE, Polley DB (2019) Cellular and widefield imaging of sound frequency organization in primary and higher order fields of the mouse auditory cortex. *Cereb Cortex* 30:1603–1622.
- Ruiz A, Walker MC, Fabian-Fine R, Kullmann DM (2004) Endogenous zinc inhibits GABA receptors in a hippocampal pathway. *J Neurophysiol* 91:1091–1096.
- Saderi D, Schwartz ZP, Heller CR, Pennington JR, David SV (2021) Dissociation of task engagement and arousal effects in auditory cortex and midbrain Carr CE, King AJ, Carr CE, eds. *Elife* 10:e60153.
- Schwartz O, Simoncelli EP (2001) Natural signal statistics and sensory gain control. *Nat Neurosci* 4:819.
- Schwartz ZP, Buran BN, David SV (2019) Pupil-associated states modulate excitability but not stimulus selectivity in primary auditory cortex. *J Neurophysiol* 123:191–208.
- van der Wel P, van Steenbergen H (2018) Pupil dilation as an index of effort in cognitive control tasks: a review. *Psychon Bull Rev* 25:2005–2015.
- Vergnano AM, Rebola N, Savtchenko LP, Pinheiro PS, Casado M, Kieffer BL, Rusakov DA, Mulle C, Paoletti P (2014) Zinc dynamics and action at excitatory synapses. *Neuron* 82:1101–1114.
- Vinck M, Batista-Brito R, Knoblich U, Cardin JA (2015) Arousal and locomotion make distinct contributions to cortical activity patterns and visual encoding. *Neuron* 86:740–794.
- Vogler NW, Betti VM, Goldberg JM, Tzounopoulos T (2020) Mechanisms underlying long-term synaptic zinc plasticity at mouse dorsal cochlear nucleus glutamatergic synapses. *J Neurosci* 40:4981–4996.
- Wang C-A, Boehnke SE, Itti L, Munoz DP (2014) Transient pupil response is modulated by contrast-based saliency. *J Neurosci* 34:408–417.
- Wilkinson GN, Rogers CE (1973) Symbolic description of factorial models for analysis of variance. *J R Stat Soc Ser C Appl Stat* 22:392–399.
- Willmore BDB, Cooke JE, King AJ (2014) Hearing in noisy environments: noise invariance and contrast gain control. *J Physiol* 592:3371–3381.
- Wilson NR, Runyan CA, Wang FL, Sur M (2012) Division and subtraction by distinct cortical inhibitory networks in vivo. *Nature* 488:343–348.
- Winn MB, Edwards JR, Litovsky RY (2015) The impact of auditory spectral resolution on listening effort revealed by pupil dilation. *Ear Hear* 36:e153.
- Wu H-PP, Dyck RH (2017) Signaling by synaptic zinc is required for whisker-mediated, fine texture discrimination. *Neuroscience* 369:242–247.
- Zekveld AA, Kramer SE, Festen JM (2011) Cognitive load during speech perception in noise: the influence of age, hearing loss, and cognition on the pupil response. *Ear Hear* 32:498–510.
- Zekveld AA, Heslenfeld DJ, Johnsrude IS, Versfeld NJ, Kramer SE (2014) The eye as a window to the listening brain: neural correlates of pupil size as a measure of cognitive listening load. *NeuroImage* 101:76–86.
- Zekveld AA, Koelewijn T, Kramer SE (2018) The pupil dilation response to auditory stimuli: current state of knowledge. *Trends Hear* 22:1–25.
- Zhao S, Chait M, Dick F, Dayan P, Furukawa S, Liao H-I (2019) Pupil-linked phasic arousal evoked by violation but not emergence of regularity within rapid sound sequences. *Nat Commun* 10:4030.
- Zingg B, Chou X, Zhang Z, Mesik L, Liang F, Tao HW, Zhang LI (2017) AAV-mediated anterograde transsynaptic tagging: mapping corticocollicular input-defined neural pathways for defense behaviors. *Neuron* 93:33–47.